Atmospheric
Chemistry
and Physics
Discussions

Open Access

Vertical fluxes and atmospheric cycling of methanol, acetaldehyde, and acetone in a coastal environment

M. Yang[1], R. Beale[1], T. Smyth[1], and B. Blomquist[2]

[1]Plymouth Marine Laboratory, Prospect Place, Plymouth, Devon, UK
[2]Department of Oceanography, University of Hawaii, Honolulu, HI, USA

Correspondence to: M. Yang (reelguy@gmail.com)

Abstract

We present here vertical fluxes of methanol, acetaldehyde, and acetone measured directly with eddy covariance (EC) during March to July 2012 near the southwest coast of the UK. The performance of the proton-transfer reaction mass spectrometer (PTR-MS) for flux measurement is characterized, with additional considerations given to the homogeneity and stationarity assumptions required by EC. Concentrations and fluxes of these compounds vary significantly with time of day and wind direction. Higher values of acetaldehyde and acetone are usually observed in the daytime and from the direction of a forested park, most likely due to light-driven emissions from terrestrial plants. Methanol concentration and flux do not demonstrate clear diel variability, suggesting sources in addition to plants. We estimate air–sea exchange and photochemical rates of these compounds, which are compared to measured vertical fluxes. For acetaldehyde, the mean (1σ) concentration of 0.13 (0.02) ppb at night may be maintained by oceanic emission, while photochemical destruction outpaces production during the day. Air-sea exchange and photochemistry are probably net sinks of methanol and acetone in this region. Their nighttime concentrations of 0.46 (0.20) and 0.39 (0.08) ppb appear to be affected more by terrestrial emissions and long distance transport, respectively.

1 Introduction

Oxygenated Volatile Organic Compounds (OVOCs), such as methanol, acetone, and acetaldehyde, exist ubiquitously in the troposphere and are important for atmospheric chemistry and climate. Methanol is the most abundant oxygenated organic gas in the atmosphere and a source of carbon monoxide (Duncan et al., 2007) and formaldehyde (Millet et al., 2006). Plant growth is a large source of methanol (Guenther et al., 2000), accounting for $30 \sim 80\%$ of total emissions to the atmosphere in global models (Singh et al., 2000; Heikes et al., 2002; Jacob et al., 2005; Millet et al., 2008). Other sources include plant decay (Warneke et al., 1999), industrial emissions (as solvents,

fuel additive, antifreeze, etc, Langford et al., 2009), and atmospheric reactions. The predominant sink for methanol in the atmosphere is the reaction with the hydroxyl radical (OH), with a lifetime of ~ 10 days (Atkinson, 2000). Methanol is also removed from the planetary boundary layer (PBL) via deposition to land (Karl et al., 2004) and to the ocean surface (Heikes et al., 2002; Williams et al., 2004; Carpenter et al., 2004).

Acetaldehyde is important for the formation of ozone (O_3), HO_x radical (Singh et al., 1995), and peroxyacetyl nitrate (Roberts, 1990), the latter a stable reservoir of nitrogen oxides. While terrestrial plants are well known to emit acetaldehyde (Hurst et al., 1994; Guenther et al., 2000; Jardine et al., 2008), a recent mesocosm measurement in a Norwegian fjord suggests that the ocean could be a source as well (Sinha et al., 2007). In the updated global budget by Millet et al. (2010), hydrocarbon oxidation in the atmosphere represents the predominant source of acetaldehyde (60 %), more than three times higher than a previous estimate (Singh et al., 2004); other sources include emissions from the ocean (27 %) and terrestrial biosphere (11 %), as well as minor anthropogenic contributions. Acetaldehyde is quickly removed from air via reactions with OH, the nitrate radical, and direct photolysis, with respective lifetimes of ~ 9 h, 6 and 17 days (Atkinson, 2000).

A significant source of OH radical in the dry, upper troposphere, acetone is also a precursor to peroxyacetyl nitrate (Singh et al., 1995). Terrestrial emissions from plants (Warneke et al., 1999; Guenther et al., 2000) and atmospheric oxidations provide similar contributions to the global acetone budget (Fischer et al., 2012), while anthropogenic emission appears to be a minor source (Langford et al., 2009). Global budgets of acetone disagree on the role of the ocean. Jacob et al. (2002) suggested the ocean to be a net source of acetone, whereas Singh et al. (2004) modeled a net loss of acetone to the surface ocean, consistent with direct flux measurements from Marandino et al. (2005) over the North Pacific. Other observations over the ocean (Taddei et al., 2009) and in the mesocosm (Sinha et al., 2007) indicated the air–sea flux of acetone to be small and variable in sign. Reaction with OH and photolysis remove acetone

from the atmosphere at similar rates, resulting in a photochemical lifetime of 39 days (Fischer et al., 2012).

With developments in mass spectrometry over the last two decades, OVOC concentrations have been measured in a variety of environments (though few by the coast). The numerous sources and sinks pose considerable challenges to the characterization and modeling of OVOC cycling based on concentrations alone. Knowing the vertical transport allows emission and deposition to be distinguished from chemical transformation, which represents a significant step forward, particularly for understanding the role of the ocean. Moreover, when multiple OVOCs are measured simultaneously, commonality and difference in the sources and sinks may be inferred.

Eddy covariance (EC) is the most direct technique for measuring vertical transport in the atmosphere. Vertical flux (F) is derived by correlating fluctuations in the species of interest (x) with concurrent vertical wind velocity (w) and averaging over time ($F = \overline{w'x'}$). When measured within the surface layer of the atmosphere ($< \sim 10$ % of the PBL), the EC flux can be equated to surface flux under stationary and horizontally homogeneous conditions. Statistical measures of x in time and space, stationarity and homogeneity refer to temporal constancy during the averaging period and spatial constancy within the flux footprint, respectively. For methanol, acetaldehyde, and acetone, the stationarity criterion (i.e. steady state) should be satisfied from the perspective that their chemical lifetimes of several hours to days are much longer than the flux averaging period of typically an hour.

To capture the full continuum of atmospheric turbulence, a fast sensor (typically $f \geq 10$ Hz) is required. With a theoretical response time of < 1 s, the proton-transfer-reaction mass spectrometer (PTR-MS) has been utilized to measure OVOC fluxes in terrestrial environments with EC (e.g. Karl et al., 2001). To accommodate the lower sampling frequency of the PTR-MS when multiple compounds are simultaneously monitored, disjunct (e.g. Rinne et al., 2001; Warneke et al., 2002) and virtual disjunct (e.g. Karl et al., 2002; Spirig et al., 2005) EC variants based discrete concentration measurements have also been used, albeit with greater flux loss at high frequencies.

Compared to terrestrial emissions, air–sea fluxes of OVOCs tend to be lower in magnitude, thus challenging the instrumental sensitivity and noise. In this paper, we first discuss the optimization of the PTR-MS for EC flux measurements of methanol, acetaldehyde, and acetone, with detailed analysis of sampling error, detection limit, and high frequency flux loss. Additional attention is given to the interpretation of flux measurements with regard to the homogeneity and stationarity requirements. Lastly, we compare measured vertical fluxes to expected air–sea exchange and photochemical rates.

2 Measurement site and environmental conditions

The city of Plymouth (population of $\sim 250\,000$) is situated on the southwestern coast of the UK. Warmed by the North Atlantic Current, the region has a temperate oceanic climate and is predominantly exposed to southwesterly winds. As shown in Fig. 1, Plymouth Marine Laboratory (PML, 50°21.57′ N, 4° 08.52′ W) is located on the northern side of the Plymouth Sound, which opens to the Atlantic Ocean to the south and is fed by the River Plym from the NE and Tamar from the NW (both estuarine). The Mount Edgcombe Park, abundant with broadleaf trees and grasses, is situated $\sim 2\,\text{km}$ SW of PML and across the Tamar. Residential buildings, a ferry port, and a naval dockyard are located NW of PML, while the City Centre is to the NE.

Measurements of OVOC concentrations and winds were made from the rooftop of the PML building, which is $200 \sim 300\,\text{m}$ from the water edge (depending on direction). A parking area fenced by broadleaf trees and garden bushes occupies the $\sim 80\,\text{m}$ region immediately south of PML, with a tall hotel across the parking area severely obstructing winds from the SSE. The view is much clearer from south to west, with moderately dense, two to three-storey residential buildings covering most of the land that slopes down to the water edge. The rooftop of the PML building is about 45 m a.s.l. and 15 m above local ground. Taking 10 m to be the height of the roughness elements (e.g. houses, trees), the roughness sublayer height can be approximated

8105

as three times the height of the roughness elements, or 30 m (World Meteorological Organization, 2006). Thus the PML rooftop should be above the roughness sublayer and within the surface layer, where standard boundary layer theory applies.

For descriptions of the regional environment, we utilize continuous observations from the PML rooftop, Rame Head, and L4 buoy, all parts of the Western Channel Observatory. Meteorological parameters were measured every 5 min from a station secured on a $\sim 2\,\text{m}$ mast near the SW corner of the PML rooftop, including horizontal wind speed and direction (Mierji Meteo solid state wind sensor, MMW-005), temperature and humidity (Hygroclip S3 sensor), precipitation (Omni Instruments 6″ tipping bucket rain gauge, RG200), solar irradiance (Li-Cor pyranometer, LI-200SZ), and photosynthetically active radiation (Chelsea Instruments half-hemisphere PAR sensor). Meteorological data were also recorded every 5 min from Rame Head, a headland several km SW of PML (50° 19.03′ N, 4° 13.19′ W). Just outside of the Plymouth Sound, the autonomous L4 buoy (50° 15.0′ N, 4° 13.0′ W) is equipped with sensors that measure surface ocean parameters hourly, including chlorophyll a from fluorescence (WetLabs WQM), nitrate (Satlantic ISUS), sea surface temperature, salinity, etc.

We report here OVOC fluxes measured during selected periods between March and July 2012. Due to unusually rainy weather, high winds, and larger riverine inputs of nutrients, the "spring" bloom of phytoplankton was almost continuous during these months, with a mean chlorophyll a concentration of $\sim 1.7\,\text{mg}\,\text{m}^{-3}$. Sea surface temperature steadily warmed from approximately 10 to 15 °C, while salinity dropped from 35.2 to 35.0 psu. Under typical southwesterly conditions, the flux footprint (the area contributing to the measured turbulent fluxes) extends to $\sim 1\,\text{km}$ upwind of PML, covering both land and coastal waters.

3 Instrumentation and basic data processing

A high sensitivity PTR-MS (Ionicon Analytik) was used to measure the concentrations of selected OVOCs. The gas inlet and a 3-d sonic anemometer (Applied Technologies,

8106

In. "K" style probe) were installed near the SE corner of the rooftop of the PML building. To avoid rain droplets, the gas inlet was constructed with two funnels held together on the broadsides, sandwiching a coarse mesh. Stabilized by an aluminum rod on the exterior, the inlet pointed downwards and was located ~ 40 cm below and 30 cm in front of the sonic center (of the w component). A ~ 25 m of Perfluoroalkoxy (Teflon PFA) tubing (1/4 in. ID) connected the inlet to the PTR-MS in a laboratory two floors below. Turbulent airflow in the manifold (Reynolds number of ~ 5000) was maintained at ~ 25 standard liter per minute (SLPM) by a vacuum pump and monitored by a digital thermal mass flow meter (Bronkhorst EL-FLOW series). OVOC concentration, wind, and flow data were recorded on the same computer.

We used an internal gas standard to account for instrumental drift in the PTR-MS. Triply deuterated (d_3) methanol diluted in nitrogen (1.01 ppm, Scientific and Technical Gases Ltd) was continuously injected to the manifold at about ~ 2 m ahead of a sub-sampling "tee" for the PTR-MS via a short piece of 1/16 in. ID Fluorinated ethylene propylene (Teflon FEP) tubing. The standard flow was controlled precisely at 0.100 SLPM by a digital mass flow controller (Bronkhorst EL-FLOW series), yielding a diluted d_3 methanol concentration of ~ 4 ppb. At the "tee", another short piece of 1/16 in. ID FEP tubing was connected to a 3-way polytetrafluoroethylene (Teflon PTFE) solenoid valve (Takasago Electric, Inc.), which directed air either directly to the PTR-MS or additionally through a catalytic converter. The PTR-MS sub-sampled from the manifold at ~ 60 mL min^{-1} via ~ 1.5 m of 1/32 in. Polyether ether ketone (PEEK) tubing, which was heated to 80 °C to minimize adsorption. The residence time of air inside of the main manifold was about 2 s, and from the "tee" to the PTR-MS another ~ 2 s. A higher sub-sampling flow by the PTR-MS may slightly improve the instrument response, but resulted in unstable chamber pressure in the current setup.

3.1 Optimization of the PTR-MS for Eddy covariance

The principle of the PTR-MS was described in detail by Lindinger et al. (1998). Very briefly, from a water vapor source the instrument produces the hydronium ion (H_3O^+)

with a proton affinity (PA) of 691 kJ mol^{-1}, which in turn transfers the charge to gas molecules of higher PA. With PA of 754, 769, and 812 kJ mol^{-1}, methanol, acetaldehyde, and acetone are ionized efficiently by H_3O^+ to form ions at mass to charge ratio (m/z) of 33, 45, and 59, respectively.

High sensitivity and low noise are desirable for EC. In order to maintain H_3O^+ as the primary source ion, a low pressure in the drift tube (reaction chamber) is typically used in the PTR-MS ($2 \sim 3$ mbar), which limits the concentrations of analytes and the frequency of molecular collisions. Increasing the chamber pressure may improve sensitivity, but can also lead to more dimerization of water molecules, which at a PA of ~ 808 kJ mol^{-1} (Goebbert and Wentold, 2004) does not ionize many OVOCs efficiently. A large fraction of the m/z 33 background is due to the oxygen isotope $^{16}O^{17}O^+$, which relates to O_2^+ by the isotopic fraction of 0.076 %. The amount of O_2^+ in the system decreases with increasing humidity (de Gouw et al., 2004), implying that the m/z 33 background may be lowered by increasing H_3O^+ input. Doing so may also result in more water dimers, which can be broken by increasing the electric field or temperature in the reaction chamber. With aforementioned considerations, the following settings were typically used: drift tube pressure of 2.8 mbar, temperature of 80 °C, voltage of 700 V, and water vapor flow of 9 sccm. A substantially higher m/z 59 background was observed at chamber temperatures above 100 °C, presumably due to desorption. The electric field to charge ratio (E/N) was 112 Td at 298 K (and greater at 80 °C), high enough to avoid excessive clustering of water molecules (de Gouw et al., 2003).

OVOC Backgrounds were quantified by diverting the gas flow through a platinum catalytic converter (Shimadzu) at 350 °C for 2 min at the beginning of every hour. The converter removes organic compounds but does not significantly alter signals at m/z 21 ($H_3^{18}O^+$), 32 (O_2^+), and 37 ($H_2O \cdot H_3O^+$). For m/z 33, 45, and 59, background values were typically 0.8, 0.3, and 0.2 ppb and generally stable (derivations of concentrations are described in Sect. 3.2). Estimated as 3σ of the 2-min backgrounds over a day, the detection limits for mean concentrations of these compounds were 0.048, 0.021, and 0.016 ppb, respectively.

To maintain a high enough sampling frequency for EC, we only monitored a few OVOC species simultaneously. Related to H_3O^+ by an isotopic ratio of 500, m/z 21 was measured at a dwell time of 50 ms, following by m/z 33, 36 (d_3-methanol), 45, and/or 59 at a dwell time of 100 ms each, resulting in a total sampling frequency of 2.1 ~ 2.5 Hz. While shorter dwell times would result in faster sampling, potential gain in speed is offset by amplified instrumental noise at ppb level concentrations. On separate measuring or scan modes, m/z 32 and 37 were monitored occasionally, and represented less than 1 % and 5 % of the m/z 21 signal, respectively.

At a dwell time of 100 ms, instrumental noise is much higher than detection limit for mean concentration. Estimated as 1 σ of high rate data during a period of background, the noise levels for m/z 33, 45, and 59 were 0.21, 0.13, and 0.10 ppb, which agree with statistical errors from a counting detector and are confirmed to be white noise from the variance spectra. The PTR-MS generally performed well during this period, with H_3O^+ of 2.5 ~ 3.0 × 10^7 counts per seconds (cps). Instrument sensitivities differed among OVOCs and improved somewhat with time, partly due to varying transmission efficiencies. From an hour after three days of continuous operation, sensitivities at m/z 33, 45, and 59 were 292, 456, and 511 cps ppb^{-1}.

3.2 OVOC concentrations from PTR-MS

The PTR-MS converts the number of analyte molecules to a mixing ratio (C) through the concentration of air in the drift tube:

$$C = \frac{10^9}{[\text{air}]} \frac{1}{k_{C^+} \cdot t_{\text{drift}}} \frac{\text{cnts}_C^+}{\text{cnts}_{H_3O^+}} \frac{\text{Tr}_{H_3O^+}}{\text{Tr}_{C^+}} \tag{1}$$

The kinetic reaction rate, k_{C^+}, depends on the chemical structure (dipole moment, polarizability, etc.) of the gas molecule (Zhao and Zhang, 2004). After removing backgrounds, cnts$_{C^+}$ and cnts$_{H_3O^+}$ are the signals of C^+ and H_3O^+ in cps. $\text{Tr}_{H_3O^+}$ and Tr_{C^+} indicate the respective transmission efficiencies of the PTR-MS, which depend on ion extraction efficiency to the quadrapole, the efficiencies of the MS and of the detector

8109

(Taipale et al., 2008). Tr is mainly mass dependent, but also varies over time and from one instrument to another.

The reaction time between H_3O^+ and the analyte within the drift tube, t_{drift}, is short under our settings at only 94 μs:

$$t_{\text{drift}} = \frac{l^2}{\mu_0 U_{\text{drift}}} \frac{T_0}{T_{\text{drift}}} \frac{P_{\text{drift}}}{P_0} \tag{2}$$

Here l is the length of the chamber (9.3 cm) and μ_0 the reduced mobility (2.8 cm^2 V^{-1} s^{-1}). U_{drift}, T_{drift}, and P_{drift} are the steadily maintained drift tube voltage, temperature and pressure, T_0 and P_0 the standard temperature and pressure. The actual residence time of air through the drift tube is much longer though. Out of the 60 mL min^{-1} sub-sampling flow by the PTR-MS, roughly half goes through the drift tube, resulting in a residence time of ~ 0.1 s, which is one of the limitations to instrument frequency response.

In the field where temperature and humidity vary significantly, efficiency and performance of the PTR-MS can fluctuate as well. Thus empirical calibration factors need to be determined accurately and frequently for individual instruments using external gas standards, which is non-trivial. Alternatively, k_{C^+} and Tr are not necessary for deriving ambient concentration from an internal isotopic standard with similar molecular properties. Such should be the case for d_3-methanol, which is structurally similar to ambient methanol and only differs in mass by three amu. Analogous to how University of Hawaii measures DMS (Blomquist et al., 2010), we derive the concentration of ambient methanol (C_{methanol}) from the ratio between counts at m/z 33 and 36:

$$C_{\text{methanol}} = C_{\text{methanol,std}} \frac{\text{cnts}_{33}}{\text{cnts}_{36}} \frac{A_{36,\text{std}}}{A_{33,\text{amb}}} \tag{3}$$

Calculated from the gravimetrically determined standard gas cylinder concentration and measured mass flow dilution rate, $C_{\text{methanol,std}}$ is the mixing ratio of d_3-methanol

8110

in the manifold. Because the d_3-methanol concentration is nearly constant, we can remove counting noise from $cnts_{36}$ with a low pass filter at a cutoff frequency of 0.017 Hz. The last ratio on the right hand side (RHS) of Eq. (3) accounts for the distributions of isotopomers at m/z 33 and 36. $A_{36,std}$ indicates the isotopic ratio of m/z 36 in the gas standard cylinder, which was measured from mass scans to be 0.9925. $A_{33,amb}$ represents the isotopic ratio of m/z 33 in ambient air, which was estimated from natural abundance of elements to be 0.9860. Abundances of the deuterated isotopomer in ambient air and the undeuterated isotopomer in the standard are insignificant and neglected in this analysis.

We monitor slow drift in the PTR-MS from the ratio between ambient methanol concentrations determined from isotopic dilution and directly outputted by the instrument: $R_{33} = C_{methanol}/C_{33,PTR\text{-}MS}$. Here $C_{33,PTR\text{-}MS}$ was calculated from Eq. (1) assuming a reaction rate of $2.6 \times 10^{-9}\,\text{cm}^3\,\text{s}^{-1}$ (Zhao and Zhang, 2004) and instrument-specific transmission efficiencies. From two separate 3-day periods, the hourly averaged R_{33} ranged between 0.82 and 0.92, with a mean (1σ) of 0.87 (0.02). The use of Eq. (1) thus appears to overestimate methanol concentration by $10 \sim 20\,\%$, likely due to uncertainties and variability in k_{C^+} and Tr. Without calibration standards for acetaldehyde and acetone for this period, we first used recommended k_{C^+} from Zhao and Zhang (2004) to compute their concentrations following Eq. (1), and further corrected them for PTR-MS drift by applying the factor R_{33}. Such adjustments could introduce additional biases to mean concentrations, but should be better for preserving temporal trends. As with $cnts_{36}$ in (3), $cnts_{H_3O^+}$ was low pass filtered in Eq. (1).

3.3 Possible biases in the concentration measurements

Because of the unit m/z resolution of the PTR-MS, different compounds very close in mass are not distinguished. Such is the case at m/z 59, where propanal and glyoxal can potentially interfere with the measurements of acetone. The PA of glyoxal is $675 \sim 691\,\text{kJ}\,\text{mol}^{-1}$ according to theoretical calculations (Wróblewski et al., 2007), prob-

ably too low to be ionized effectively by H_3O^+. While the detection of propanal should be more efficient because of its greater PA at $784\,\text{kJ}\,\text{mol}^{-1}$, Warneke et al. (2003) suggested that due to its short atmospheric lifetime ($\sim 9\,\text{h}$), the background concentration of this industrially emitted compound should be low away from source.

Northway et al. (2004) suggested that heterogeneous reaction with O_3 on the inlet wall could lead to acetaldehyde formation, an artifact likely more severe for stratospheric air and for gas chromatography (Apel et al., 2008). Given our high manifold flow rate and short residence time, a large inlet-related artifact seems unlikely. O_3 concentration measured at Rame Head was usually below 20 ppb, with a diurnal fluctuations of $4 \sim 5$ ppb for SW winds. The lack of clear correlation between acetaldehyde and O_3 as well as the low magnitude and range in O_3 also do not support substantial heterogeneous production of acetaldehyde. Furthermore, in theory any artificially produced acetaldehyde in the inlet should not be correlated with vertical wind velocity. Nevertheless, with potential artifacts and without specific internal standards, our measured concentrations of acetone and acetaldehyde are more uncertain.

3.4 General trends in OVOC concentrations

Concentrations of methanol, acetaldehyde, and acetone varied substantially due not only to local production and destruction, but also horizontal advective and turbulent transport. Figure 2 shows the OVOC concentrations vs. wind direction for $6 \sim 8$ June, when a large low-pressure system passed by Plymouth, resulting in heavy precipitation at times and wind gusts up to $20\,\text{m}\,\text{s}^{-1}$. High winds and wet deposition likely reduced the PBL loadings of these OVOCs upwind, allowing observed concentrations to be more reflective of local changes. We separate concentrations to day (approximately one hour after sunrise to one hour before sunset) and night (one hour after sunset to one hour before sunrise). For methanol, the nighttime concentration was ~ 0.5 ppb and uniform with respect to wind direction. During the day, however, methanol concentration ranged from ~ 0.5 ppb to an order of magnitude higher; the latter generally

occurred when winds were from the NW, possibly related to anthropogenic activity. Nighttime concentrations of acetaldehyde and acetone were also relatively steady at ~ 0.1 and 0.4 ppb, independent of wind direction. In contrast, daytime concentrations of acetaldehyde and acetone were $2 \sim 3$ times the nighttime values, peaking from WSW. The directional dependence suggests that the higher daytime values were related to surface sources rather than widespread photochemical production in the atmosphere.

Methanol generally showed more fluctuations on short timescales than acetone, likely due to greater strength and spatial heterogeneity of methanol sources. This is clearly visible during $3 \sim 4$ March when winds were largely from the SW (Fig. 3). Despite similar mean concentrations of ~ 0.4 ppb, σ in methanol concentration was about five times greater than that of acetone. If the fluctuations in concentration were mainly from vertical turbulent transport, methanol flux should be several times larger than acetone flux, which we show later to be the case. OVOC concentrations were often elevated when winds were weak (e.g. 03:00 LT to 06:00 LT on 4 March). A shallow nocturnal boundary layer during this period probably concentrated these gases.

A time series of acetaldehyde concentration during 15 June is shown in Fig. 4 along with solar irradiance. Whitecapping was clearly visible over the Plymouth sound on this day with strong winds ($\sim 11 \, \text{m s}^{-1}$) from the SSW. Atmospheric dimethylsulfide (DMS) concentration was also detected by the PTR-MS, which confirmed the marine influence. Consistent with previous diel cycle observations (e.g. Bandy et al., 1996; Yang et al., 2009), DMS concentration decreased in the afternoon when photochemical destruction outpaced sea-to-air emission, until a few hours before sunset. Contrastingly, acetaldehyde concentration generally increased with solar flux.

Crudely, we can consider the nighttime concentrations of OVOCs from the wind sector of $180 \sim 270°$ to be their "baselines" for North Atlantic air, which for methanol, acetaldehyde, and acetone were 0.46 (0.20), 0.13 (0.02), and 0.39 (0.08) ppb (mean and 1σ from March to July). This methanol concentration is similar to previous aircraft measurements over the Pacific (Singh et al., 2004) and ground-based observations from the marine sector at Mace Head, on the west coast of Ireland (Lewis et al., 2005). The

8113

acetone concentration above is also comparable to those measured from the Tropical Atlantic (Williams et al., 2004) and Mace Head (Lewis et al., 2005), but lower than values reported by Marandino et al. (2005) north of 25° N in the Atlantic. Any inlet-related artifact aside, 0.13 (0.02) ppb of acetaldehyde is somewhat lower than previous nighttime observations by Zhou and Mopper (1993) from the Caribbean and by Lewis et al. (2005).

4 Eddy covariance flux calculations

Undisturbed atmospheric turbulence is critical for the EC method. The rooftop is admittedly not an ideal location because of potentially large distortion of airflow by the building superstructure. To best capture SW winds, we extended the sonic anemometer horizontally beyond the building wall by ~ 2 m (to the south). Wind velocities in 3-axis (u, v, w) and temperature (T_s) were recorded by the anemometer at a frequency of 10 Hz. In our set up, u was along the NS direction, perpendicular to the wall, v along the EW direction, and w positive upwards, such that a positive flux indicates an upward transfer from the surface. The sonic anemometer temperature (T_s) was corrected for humidity to yield the air temperature (T_a). A standard double rotational correction was applied to u, v, and w to account for the streamline of airflow over the building superstructure. After rotation, both v and w averaged zero, while u aligned with the mean horizontal wind.

The severity of wind distortion is reflected in the tilt angle from the second rotation, which typically ranged from $\sim 10°$ for W winds to $\sim 20°$ for SW winds, as air was forced upwards when encountering the building. Distortion of airflow is also evident from the ratios in the variance spectra (S) between u, v, and w after rotation. In the inertial subrange ($> \sim 1$ Hz), both $S_w(f)/S_u(f)$ and $S_v(f)/S_u(f)$ should be $\sim 4/3$, which were indeed the case for westerly winds, implying minimally distorted flow. For SW winds, though, while $S_w(f)/S_u(f)$ remained at 4/3, $S_v(f)/S_u(f)$ was generally higher at ~ 1.5, indicating a greater flow distortion (increased variance) in the direction orthogo-

8114

nal to the mean horizontal wind. Fortunately, the computation of scalar fluxes only requires w, not u and v. Thus disturbance in the horizontal probably did not significantly bias OVOC fluxes, but may have contributed additional scatter. Despite the non-ideal measuring location, wind direction from the sonic anemometer generally shows good agreement with the solid-state sensor from the PML rooftop and with the mechanical (cup) anemometer from Rame Head. Due to an instrument fault, one or two channels of the sonic anemometer sensor often outputted corrupted data during heavy rain. No EC flux could be derived in such periods; however, mean wind speeds from the Rame Head were used in the evaluation of OVOC concentrations.

4.1 Sensible heat and momentum fluxes

Sensible heat flux ($Q_H = \overline{w'T_a'}$) and momentum flux ($\tau = \rho\overline{w'u'}$) were calculated hourly using data from the sonic anemometer, with ρ being the ambient air density. As expected, Q_H generally followed the trend in temperature, higher during the day than at night. Lower Q_H was observed for SSW winds over the Plymouth Sound than for W winds over more land. Greater Q_H in the latter case was likely related to concrete buildings and asphalt surfaces within in the flux footprint, which absorb and emit heat more quickly than water. The absolute sampling error in Q_H was estimated following Fairall et al. (2000) and amounted to $\sim 30\%$ for the daytime.

Momentum flux was generally negative, indicating a transfer of stress to the surface and confirming the expected logarithmic wind profile. The friction velocity, $u_* = (-\tau/\rho)^{1/2}$, demonstrated a near linear relationship with wind speed, but was larger than what is expected over the ocean, likely because of the greater momentum roughness length (z_0) within the flux footprint. Categorizing the region from PML to the water edge under class 6 for terrain roughness scale (World Meteorological Organization, 2006), z_0 is on the order of 0.5 m. It is uncertain though how much the enhanced momentum transfer measured affected the transfer of scalars, such as heat and OVOCs.

To determine atmospheric stability, the Obukhov length was calculated as $L = -u_*^3/[\kappa(g/\theta_v)/Q_H]$. Here κ is the von Karmon constant, g the gravitational acceleration, and θ_v the potential temperature. We take the vertical displacement as half of the height of the roughness elements (5 m) and reference height z the measurement height above displacement (~ 40 m). The Monin-Obukhov stability parameter (z/L) varied from -1 (unstable) to slightly positive (weakly stable) in our observations, with zero indicating neutrality.

4.2 OVOC fluxes

Precise timing is required for EC to prevent a loss of flux. While the anemometer data were essentially instantaneous, several seconds were required for air to travel from the inlet to the PTR-MS, through the drift tube, and be detected. Additional time lag may occur because of spatial separation between the wind sensor and the inlet and inaccuracy of the computer clock. The most direct method to account for the total time shift is to perform a lag correlation analysis between OVOC concentration and w.

We linearly interpolated winds from 10 Hz to match the sampling frequency of the PTR-MS at $2.1 \sim 2.5$ Hz. Lag correlations between w and all three OVOC species were calculated hourly within a ± 15 s window. A sharp peak in correlation coefficient indicated a clearly detected flux, with the time of maximum correlation corresponding to the total lag. Methanol flux was always easily detectable, yielding the most robust lag time estimates at -4.5 ± 0.5 s, consistent with given flow rates. Analogous analyses between w and acetaldehyde or acetone demonstrated clear peaks when the fluxes were large, with lag times consistent with those from w: methanol. For other hours, lag times from the methanol analysis were used for acetaldehyde and acetone flux calculations. After synchronization, OVOC fluxes were processed in hourly blocks. Periods of rapid change in wind direction or large spikes in concentrations were excluded if they occurred at the beginning or end of the analysis window. We did not apply a despiking algorithm on the concentrations prior to flux calculation, but instead used hourly statistics for quality control, as described in Sect. 4.4.

To examine the robustness of measured fluxes and determine the dominant flux timescale, we compare the cospectra methanol, acetone, and acetaldehyde to the cospectrum of sensible heat. Each was normalized ny the respective flux and usually averaged over a few hours of steady winds to reduce noise. An example is shown in Fig. 5. Measured coincidentally during and after trimming of garden bushes in the upwind region, the OVOC fluxes were exceptionally large and the cospectra well-defined. The four cospectra agreed with each other and demonstrated the expected shape from atmospheric turbulent transport (Kaimal et al., 1972). During our observational period, the methanol cospectrum was almost always well-defined and similar to that of sensible heat. Cospectra of acetaldehyde and acetone were noisier though because of the lower magnitudes of the fluxes.

4.3 Sampling error and precision in OVOC flux

Due to stochastic randomness in turbulent eddies, flux needs to be averaged over a long enough time period (T) to be statistically representative. We estimate the absolute (random) sampling error in OVOC fluxes (ΔF_C) following Blomquist et al. (2010):

$$\Delta F_c = \frac{a\sigma_W\sigma_{Ca}}{\sqrt{T/\tau_{WCa}}}\left[1 + \frac{\varphi_{Cn}}{4\sigma_{Ca}^2\tau_{WCa}}\right]^{1/2} \tag{4}$$

An expansion of the formulae from Fairall et al. (2000), ΔF_C in Eq. (4) arises from both natural variability (first term on RHS) and instrumental noise (second term on RHS). The natural variance in the OVOC concentration (σ_{Ca}^2) is taken to be the second point in the autocovariance function. The noise contribution relates to the white noise of the instrument (φ_{Cn}), which was about $0.02 \sim 0.03\,ppb^2\,Hz^{-1}$. The integral timescale (τ_{WCa}) increases with sampling height and decreases with wind speed:

$$\tau_{WCa} = b\frac{z}{u}[\min(5, \max(0.5, (1 + 0.6z/L)))]^{-1} \tag{5}$$

ΔF_C is similar for neutral and unstable cases but becomes much greater for a stable atmosphere. Using empirical values of 1 and 2.8 for a and b (C. Fairall, unpublished data), the flux sampling error for methanol was on the order of $\sim 50\,\mu moles\,m^{-2}\,d^{-1}$, or $\sim 30\,\%$ of the mean flux. ΔF_C decreased to $\sim 30\,\mu moles\,m^{-2}\,d^{-1}$ ($\sim 20\,\%$) at winds above $10\,m\,s^{-1}$ but increased substantially in calm conditions. For acetaldehyde and acetone, the flux errors were on average ~ 10 and $\sim 16\,\mu moles\,m^{-2}\,d^{-1}$, or $\sim 70\,\%$ and $50\,\%$ of the mean respective fluxes. Except for in pollution plumes, natural variance was several times smaller than white noise, but contributed to majority ($\sim 80\,\%$) of the sampling error in Eq. (4), which caused ΔF_C to be greater for methanol than for acetaldehyde and acetone. As such, lowering instrumental noise alone may not substantially reduce flux uncertainty.

Spirig et al. (2005) estimated the precision in EC flux from variability of the covariance at a time lag far away from the true lag. We follow the same strategy and calculate "null" OVOC fluxes at an implausible lag time ($+15\,s$). From several hours of steady winds, σ of the null fluxes were ~ 8, 5, and $4\,\mu moles\,m^{-2}\,d^{-1}$ for methanol, acetaldehyde, and acetone, increasing with natural variance as well as instrumental noise. Estimated as 3σ, the detection limits of our system with respect to these compounds were ~ 24, 15, and $12\,\mu moles\,m^{-2}\,d^{-1}$ for hourly measurements, on the same order as ΔF_C.

4.4 Quality control filters

Over spatially homogenous terrain and under stationary conditions, horizontal terms in the conservation equation approach zero, allowing measured turbulent transport at height to be equated to surface flux. In reality, these criteria were strictly never satisfied at our location due to variable seascapes and changing meteorological conditions. As a result, we rely on quality control filters based on hourly statistics in winds, turbulence, and OVOC concentrations to limit errors arising from nonstationarity and inhomogeneity. Valid heat fluxes must satisfy all of the following: σ in wind direction less than 60°, ratio of horizontal wind variance to wind speed less than $1\,m\,s^{-1}$, z/L less than 0.05,

σ_W/u_* between 1.0 and 1.6, Q_H over $-20\,\mathrm{W\,m^{-2}}$, and the difference between covariance and cospectrum-integrated Q_H less than 20 % (for the daytime).

Schulz and Sanderson (2004) used σ in wind direction and the horizontal wind variance as stationarity criteria for analyzing shipboard data. We use the same indicators but relax the thresholds given the more variable winds in our region. Based on EC measurements of DMS over the open ocean, Yang et al. (2011) showed greater uncertainty and possible underestimation of the flux under stable conditions ($z/L < 0.05$), when turbulence becomes more intermittent. A measure of the relative importance between convective and mechanically driven turbulence, σ_W/u_* is expected to be around 1.3 for the surface layer. We interpret σ_W/u_* far from 1.3 to indicate severe flow distortion or suppressed turbulence. Lastly, the integral of the cospectrum over all measured frequencies is mathematically equivalent to the direct covariance. Methodological errors are implied when the covariance and cospectrum-integrated fluxes differ substantially. About 70 % of the hourly heat flux measurements pass the aforementioned filter. Because of the occurrence of stable nocturnal boundary layer, more daytime flux measurements remain valid.

For OVOC fluxes, we require Q_H to be valid, and place additional filters on short-term variability and long-term trend in OVOC concentrations. Calculated as the hourly σ divided by mean concentration, large short-term variability reflects changes in concentration due to processes other than vertical transport, such as advection of a plume or horizontal turbulent flux arose from inhomogeneity. Nominal criteria are less than 0.8 for methanol and acetaldehyde and less than 0.4 for acetone, the latter a result of its smaller fluctuations. Long-term variability is quantified by the temporal change in OVOC concentration (hourly) normalized to the mean, with a threshold set to $0.3\,\mathrm{h^{-1}}$ for all OVOCs. About half of the measured OVOC fluxes pass all aforementioned criteria.

Following Spirig et al. (2005) and Schulz and Sanderson (2004), we further evaluate the stationairty assumption through the ogive analysis (Oncley, 1989). The ogive (Og) is calculated as the cumulative sum of the cospectrum (Co) from the lowest measured

8119

frequency (f_L) to the Nyquist frequency (f_N):

$$\mathrm{Og}(f) = \int_{f_L}^{f_N} \mathrm{Co}(f)\mathrm{d}f \tag{6}$$

For ease of comparison, dividing Eq. (6) by the flux yields a normalized Og of 1 at f_N. Ogives from two periods are shown in Fig. 6. On 4 July, strong surface emissions, steady winds, and well-defined cospectra (Fig. 5) led to the expected "S" shape for all ogives. On 31 May, however, rising winds led to increasing concentrations in acetone and acetaldehyde, but not methanol, which are reflected as elevated Og for acetone and acetaldehyde at low frequencies. While it might be easier to satisfy the stationarity requirement by computing flux at shorter intervals (e.g. 15 min), $\sim$ hourly averaging is beneficial for resolving OVOC transport at the given instrumental noise.

4.5 Quantifying flux loss

Due to sampling limitations, the entire turbulence spectrum may not have been captured by our system. Particularly at high frequencies, flux loss occurs as a result of limited instrument response, which is evident in Fig. 5. The drop off to zero is abrupt in the OVOC cospectra at ~ 1 Hz, whereas a "tail" remained in the sensible heat cospectrum up to 5 Hz. While all four cospectra peaked at ~ 0.07 Hz, OVOCs were normalized to attenuated values and thus demonstrated higher maxima than heat. In addition, OVOCs are often considered "sticky" due to their propensity to adsorb to the tubing wall, which could limit instrument response.

We estimate flux loss in two ways – from the instrument frequency response and based on concurrent heat flux measurements. Bariteau et al. (2010) parameterized flux loss through tubing using the instrument response time (τ_c), defined as the number of seconds for a pulsed signal to fall to 1/e of its original value. An empirical filter function is given the form: $H(f) = [1 + (2\pi f \tau_C)^2]^{-1}$. True turbulent flux is then adjusted from mea-

8120

sured flux by the factor $H(f)^{-1/2}$. While the theoretical response time of the PTR-MS is quoted to be 0.1 s, the actual response time depends on sampling frequency and flow rate. In earlier laboratory tests with identical flows, we injected d_3-methanol standard at the tip of the inlet and observed the decline of the signal once the standard was turned off. At sampling frequencies of 2.1 ∼ 2.5 Hz, τ_c was estimated to be 1.0 ∼ 0.8 s – same as the respective f_N. Inserting τ_c to the filter function and applying it to the measured cospectra resulted in flux corrections on the order of 10 ∼ 20 %, with half power frequencies at ∼ 0.18 and 0.22 Hz.

Further loss in OVOC flux could occur as a result of spatial separation between the gas inlet and the sonic anemometer (Moore, 1986). Thus we compare the transport of OVOCs (which is attenuated in high frequencies) to the transport of heat (which should not be significantly attenuated). Instead of matching the cospectra, we find the ogive approach for estimating high frequency attenuation (Spirig et al., 2005; Ammann et al., 2006) to be more repeatable. Averaged over a few hours of relatively constant winds to reduce noise, Og of OVOC usually reached 1 at a lower frequency than the heat ogive, implying high frequency attenuation. We scaled the OVOC Og to the heat Og up to a frequency where attenuation was not yet significant (usually ∼ 0.05 Hz). The corrected OVOC Og at f_N then indicated the magnitude of flux attenuation. Three examples of the ogive analysis for methanol are shown in Fig. 7. On 30 May, 6 June, and 15 June, the wind speeds were about 5, 8, and 11 m s^{-1}, with stability parameter z/L at −0.70, −0.16, and −0.05, respectively. The estimated loss in flux at a sampling rate of 2.1 Hz was ∼ 7, 17, and 24 % for these three days, increasing with wind speed and stability, which is caused by greater flux contribution from high frequencies with increasing mechanically driven turbulence. Losses in flux for methanol, acetaldehyde, and acetone based on this analysis are similar to each other and comparable to the filter function estimates, suggesting insignificant roles of adsorption and sensor separation.

Recently, Geissbaum and Schmidt (2009) examined the effect of flow distortion on turbulent measurements from a location of severe wind obstruction (e.g. a heavily in-

strumented tower). Through 3-D fluid dynamic modeling and large eddy simulation, they found that the double rotation correction for streamline flow could lead to over-estimation of scalar fluxes up to 15 %. Such a bias would be similar in magnitude to our frequency-related flux loss, but opposite in direction. Given the flow distortion at our site, we decide to present OVOC fluxes "as measured", rather than applying any correctional factors. Nevertheless, the methods discussed above should be useful for correcting measurements at more ideal locations. Overall, we see that most of turbulent transport can be captured by sampling at a relatively modest rate of > 2 Hz. One benefit of measuring at ∼ 45 m compared to closer to the surface is that a greater contribution to flux comes from lower frequencies, which are better captured by our system.

5 Results and discussion

Three time periods of flux measurements are shown here to demonstrate the application of quality control filters and the variability in OVOC fluxes. The first is taken from 30 May to 1 June, during three days of largely sunny weather and light westerly breeze. Figure 8 shows times series of wind direction and solar irradiance (a), temperature and sensible heat flux (b), methanol concentration and flux (c), acetaldehyde concentration and flux (d), and acetone concentration and flux (e). We have included fluxes both accepted and rejected by the quality control filters, with error bars corresponding to the random flux sampling errors (as with subsequent flux plots). With winds coming over land, methanol concentration was high during this period. Many hours did not pass the quality control filters because of excessive variability in wind direction (usually when winds ceased) or rapidly varying concentrations. Within remaining valid data, acetaldehyde flux followed the trend of Q_H, and was slightly positive at night (emission), while acetone flux was usually positive but also occasionally negative (deposition).

The second example is taken from 6 ∼ 8 June (Fig. 9), the same period as Fig. 2. Wind direction was fairly steady from WSW on 6 June and W on 8 June, with mostly sunny weather. Heavy rain fell for most of 7 June and the early morning of 8 June,

corrupting sonic anemometer data. Acetaldehyde flux was always positive, ranging from $\sim 30\,\mu\mathrm{moles\,m^{-2}\,d^{-1}}$ during the day to lower values in the early morning or late afternoon. Acetone flux was positive under strong sunlight ($\sim 60\,\mu\mathrm{moles\,m^{-2}\,d^{-1}}$), but near zero otherwise. The rapid declines in fluxes of sensible heat, acetaldehyde, and acetone on the afternoon of 6 June were probably due to not only diminishing solar irradiance at the end of the day, but also a shift in wind direction towards the south. Methanol concentration varied more than an order of magnitude and changed markedly with wind direction. The rapid build up and large spikes in methanol concentration on 8 June, when acetaldehyde and acetone concentrations only increased gradually, suggests pollution sources for the former.

Lastly, Fig. 10 shows the times series during $15 \sim 16$ July. Wind speeds were $\sim 8\,\mathrm{m\,s^{-1}}$ the first day and increased to $\sim 11\,\mathrm{m\,s^{-1}}$ on the second day, while the weather changed from sunny to mostly cloudy with intermittent showers. A rapid shift in winds occurred from 05:00 LT to 08:00 LT on 16 July, accompanied by a 2-degree drop in air temperature and doubling of methanol and acetone concentrations, whereas acetaldehyde concentration was less affected. EC fluxes during such hours of rapid changes were rejected, as were hours with large spikes in OVOC concentrations (e.g. $14:00 \sim 16:00$ LT on 16 July for acetaldehyde). On average, acetaldehyde flux was slightly positive, while acetone flux was near zero for the nighttime. Methanol flux did not demonstrate a clear diel difference, but varied with wind direction.

5.1 General trends in OVOC fluxes

In Fig. 11, we plot hourly fluxes of methanol, acetaldehyde, and acetone vs. wind direction. All valid hours from March to July are included here, which are further separated into day and night. Methanol flux was large and always positive, peaking in the direction of WSW. Somewhat higher emissions (mean $\pm 1\sigma$) were observed during the day ($235 \pm 110\,\mu\mathrm{moles\,m^{-2}\,d^{-1}}$) than at night ($169 \pm 92\,\mu\mathrm{moles\,m^{-2}\,d^{-1}}$) over all wind directions considered; though from the direction of the Plymouth Sound (SSW) only, flux was lower and also similar between day and night ($153 \pm 72\,\mu\mathrm{moles\,m^{-2}\,d^{-1}}$). For acetalde-

8123

hyde, much higher flux was observed during the day ($23 \pm 15\,\mu\mathrm{moles\,m^{-2}\,d^{-1}}$) than at night ($6 \pm 5\,\mu\mathrm{moles\,m^{-2}\,d^{-1}}$) for WSW winds; however, no significant diel difference was observed for SSW winds only based on limited data ($8 \pm 6\,\mu\mathrm{moles\,m^{-2}\,d^{-1}}$). Acetone flux was quite variable but generally larger during the day ($43 \pm 46\,\mu\mathrm{moles\,m^{-2}\,d^{-1}}$). With exception of one hour, nighttime acetone fluxes varied between generally $-10\,\mu\mathrm{moles\,m^{-2}\,d^{-1}}$ and $20\,\mu\mathrm{moles\,m^{-2}\,d^{-1}}$. We can also compare Fig. 11 to the OVOC concentration distributions in Fig. 2, even though the sampling times considered are not identical. For acetaldehyde and acetone, higher fluxes during the day than at night agree with the respective patterns in concentrations. For methanol, significant flux at night is consistent with observation of substantial nighttime concentration. Wind directions corresponding to maxima fluxes largely coincide with maxima in concentrations, suggesting that the higher daytime concentrations were at least in part driven by greater emissions.

Diel patterns in OVOC emissions from terrestrial sites have been reported previously based on direct flux measurements (e.g. Karl et al., 2001; Davison et al., 2009) and observed concentrations (e.g. Hu et al., 2011). Here we demonstrate the relationship between acetaldehyde/acetone flux and the sensible heat flux (Fig. 12 and 13). From the direction of SW to W, a fairly high degree of correlation exists between acetaldehyde flux and Q_H ($r^2 = 0.72$); in contrast, no correlation is seen in the direction of SSW over the Plymouth Sound. A positive correlation also exists between acetone flux and Q_H, in particular when winds were from the W ($r^2 = 0.52$). The same analysis between methanol and Q_H yielded a much weaker correlation ($r^2 = 0.22$), which is not shown here.

Temperature and light dependent, OVOCs are primarily emitted from plant growth in the daytime during photosynthesis, while at night emissions should be shut off due to stomatal control (e.g. Nemecek-Marshall et al., 1995). Given the terrestrial plants present in our flux footprint, positive correlations between OVOC fluxes and sensible heat flux are unsurprising. Interestingly, for acetaldehyde flux the degree of correlation is higher with Q_H than with temperature, solar flux, or PAR alone. At night, there

8124

can still be minor emissions of OVOCs from decaying plants, such as leaf litter. Millet et al. (2010) estimated plant decay to account for about a quarter of the terrestrial plant emission of acetaldehyde globally. Millet et al. (2008) and Jacob et al. (2002) suggested similar contributions by decaying plants to terrestrial emissions of methanol and acetone, respectively. Applying this fraction to our daytime fluxes from SW to W yield $\sim 6\,\mu\text{moles}\,\text{m}^{-2}\,\text{d}^{-1}$ of acetaldehyde and $11\,\mu\text{moles}\,\text{m}^{-2}\,\text{d}^{-1}$ of acetone, similar to the mean nighttime fluxes. For methanol, 1/4 of the daytime flux only amounts to $\sim 60\,\mu\text{moles}\,\text{m}^{-2}\,\text{d}^{-1}$, less than half of the nighttime value. Thus there appear to be other sources of methanol in addition to terrestrial plants, which would also explain the lower correlation between methanol flux and Q_H. Since our measurements were made during the growing season, actual contributions from decaying plant matter might be lower.

5.2 Flux and concentration footprints

To better understand the relationship between fluxes and concentrations, we must consider their source regions, which are not identical here. The flux footprint describes the horizontal scale (source area) and relative contribution (probability distribution) to the turbulent flux. Elliptical in shape and aligned in the upwind direction from the sensor, the flux footprint varies with measurement height, surface roughness, and atmospheric stability (Horst and Weil, 1992). We estimate our flux footprint using the simple parameterization from Kljun et al. (2004), which relies on u_* and σ_w to describe the stability dependence. The following nominal model inputs were used: z of 40 m, PBL of 1 km, z_0 of 0.5 m, u_* of $0.7\,\text{m}\,\text{s}^{-1}$, and σ_w of $0.9\,\text{m}\,\text{s}^{-1}$. The approximate footprints covering cumulative flux contributions of 60 % and 90 % are shown in Fig. 1 for SW winds. The far edge of the footprint at 90 % is about 1 km away from PML, with the peak contribution occurring at ~ 350 m upwind of the sensor, near the waterfront. Lowering σ_W/u_* to 1.0 (more shear) lengthens the footprint by ~ 20 %, while increasing σ_W/u_* to 1.6 (more convection) shortens it by ~ 20 %. With winds from SSW to SW, the relative areal contributions from land and water are on the order of 30 % and 70 %, respectively. Measured

flux then represents the net turbulent transport from within the footprint, or a spatial average of all emissions and depositions.

The source area for concentration (or the concentration footprint) is much larger than the flux footprint (Wilson and Swaters, 1990; Schmid, 1994). Thus changes in mean concentrations at the source can be detected at a long distance away, where turbulent flux contribution has already vanished. Large amounts of OVOCs are almost certainly emitted from terrestrial plants in the Mount Edgcombe Park. At ~ 2 km away from PML, the park probably lies beyond the flux footprint, but is well within the concentration footprint. Thus OVOC concentrations for SW winds likely reflect emissions within the flux footprint and also from Mount Edgcombe, which are then advected to our sensor.

5.3 Expected air–sea transfer

To put our measured fluxes in perspective, we use gas exchange parameterizations to approximate the expected air–sea flux based on measured atmospheric concentrations at PML (C) and waterside concentrations (C_w) from near the Plymouth Sound: $K_a\,(C_W/\alpha - C)$. Here α is the dimensionless solubility, and K_a the total transfer velocity from the air perspective. Following the two-layer model (Liss and Slater, 1974), K_a is expanded to individual transfer velocities through the airside and waterside (k_a and k_w, respectively). For simplicity, we calculate k_a from Duce et al. (1991) and k_w from the NOAA COARE gas transfer model (Fairall et al., 2003, 2011) with a constant of 1.3 for direct transfer and zero for bubble-mediated transfer. At 14 °C and a wind speed of $8\,\text{m}\,\text{s}^{-1}$, K_a for methanol, acetaldehyde, and acetone are on the order of 3100, 2100, and $2300\,\text{cm}\,\text{h}^{-1}$, respectively.

Since waterside OVOC concentrations were not measured concurrently to the EC fluxes, we refer to near surface (~ 5 m) observations from weekly sampling at the L4 station in 2011. As described in detail by Beale et al. (2011), seawater OVOC concentrations were analyzed with the same PTR-MS coupled with a membrane-inlet. For the year 2011, the mean (maximum) seawater concentrations of methanol, acetaldehyde, and acetone from March to July were 50 (68) nM, 9 (19) nM, and 7 (10) nM. We also

examined the possible influence of the River Tamar by taking water samples at a depth of ~10 cm along a transect from the mouth of the Plymouth Sound to inside of the estuary on the morning of 16 June 2012. Measured at a period of outgoing tide, OVOC concentrations were broadly similar to the springtime values in 2011 and did not show any enhancement inside of the estuary compared to the Plymouth Sound.

With nighttime atmospheric concentrations of 0.46, 0.13, and 0.39 ppb and the above mean (maximum) waterside values, the expected air–sea fluxes are −10 (−9), 5 (13), and −5 (−4) μmoles m^{-2} d^{-1} for methanol, acetaldehyde, and acetone, respectively. The air–sea flux of methanol is much smaller in magnitude and opposite in sign to the measured vertical flux, likely because deposition to the sea surface was overwhelmed by large terrestrial emissions. The expected oceanic emission of acetaldehyde is consistent with the measured flux from the SSW. Though given the heterogeneities within the flux footprint, the possibility of coincidental agreement cannot be ruled out. Lastly, the small deposition flux of acetone predicted is consistent with EC measurements from Marandino et al. (2005) and the recent model estimate from Fischer et al. (2012). While our mean nighttime flux of acetone was slightly positive, negative flux was also occasionally observed and on the order of −5 μmoles m^{-2} d^{-1}.

5.4 Photochemistry and local OVOC cycling

In addition to surface emission and deposition, OVOCs are also produced in situ from oxidations of precursors and photochemically destroyed in the atmosphere. Here we crudely estimate their photochemical rates and compare them to observed vertical fluxes and time rate of change in concentrations. The principal atmospheric source of methanol is the reactions of methyl peroxy radical with itself and with other peroxy radicals (Madronich and Calvert, 1990). Acetaldehyde is mainly formed from direct oxidations of alkanes including ethane, propane, *n*-butane, as well as propene and ethanol by the OH radical (Millet et al., 2010), with oxidation of isoprene through intermediates being a minor source. Acetone is produced from OH oxidation of propane and C4 ~ C5 isoalkanes, including mainly *i*-butane and *i*-pentane (Singh et al., 1994).

8127

For precursor concentrations, we use 1, 0.1, 0.03, 0.02, and 0.02 ppb for ethane, propane, *n*-butane, *i*-butane, and *i*-pentane from springtime measurements at Mace Head (Grant et al., 2011). From the same location, Salisbury et al. (2001) reported ~0.02 ppb of propene and 4 ppt of peroxy radical (an upper limit of organoperoxy radical) in the spring from the ocean sector. Lastly, from mass scans with the PTR-MS, we observed concentrations of ethanol and isoprene on the order of 0.1 and 0.04 ppb, respectively. For simplicity, we assume a diel average OH concentration of 10^6 molecules cm^{-3} and the kinetic reaction rates with OH from Sander et al. (2006). The molar yields from precursor compounds are taken from Millet et al. (2008) for methanol, Millet et al. (2010) for acetaldehyde, and Jacob et al. (2002) for acetone.

The estimated methanol production rate from peroxy radical reactions is only 0.009 ppb d^{-1}, much lower than the methanol destruction rate by OH at −0.078 ppb d^{-1} (for 1 ppb of methanol). The total photochemical production of acetaldehyde is about 0.06 ppb d^{-1}, several times lower than the OH destruction of acetaldehyde at −0.28 ppb d^{-1} (for 0.2 ppb of acetaldehyde). Photochemical production of acetone is around 0.014 ppb d^{-1}, while its loss to OH is also slow at −0.007 ppb d^{-1} (for 0.5 ppb of acetone). Using the absorption cross-section and quantum yield from Blitz et al. (2004) and the spectral actinic flux from the NCAR Tropospheric Ultraviolet and Visible (TUV) Radiaiton Model (http://cprm.acd.ucar.edu/Models/TUV/), we estimate a photolytic loss of acetone of −0.011 ppb d^{-1}, resulting in a net in situ acetone production of −0.004 ppb d^{-1}. The long photochemical lifetime and limited air–sea flux suggest greater importance of horizontal advection in the acetone budget.

Assuming a PBL of 1 km, photochemistry removed methanol, acetaldehyde, and acetone at −3, −8, and −0.2 μmoles m^{-2} d^{-1}. In comparison, we measured daytime emission rates on the order of 200, 20, 40 μmoles m^{-2} d^{-1} for these compounds, respectively. For all three OVOCs, changes in emissions often did not correspond to changes in their PBL loadings. In addition to advection, a part of this apparent imbalance may be explained by the significant horizontal turbulent transport along the mean wind direction ($\overline{u'C'}$), which was usually on the same order as the vertical flux.

8128

Compared to the cospectrum of the vertical flux, that of the horizontal turbulent flux was shifted towards lower frequencies, as shown in Fig. 14. The non-zero $\overline{u'C'}$ implies substantial horizontal flux divergence as a result of spatial inhomogeneity, which leads to additional variance in concentration. Such natural variability not only contributes to the random flux sampling error in the vertical and necessitates a longer averaging time (Blomquist et al., 2012), but also could potentially bias the EC measurement judging from studies of sensible heat (Panin et al., 1998; Raabe et al., 2002).

6 Conclusions

In this paper, we characterized the performance of the PTR-MS for measuring fluxes of a few OVOCs concurrently with direct eddy covariance. Random sampling errors and detection limits for hourly fluxes were similar in magnitude; both were determined not only by instrumental noise, but also by natural variability in concentrations as well as environmental conditions. At a sampling rate of $2.1 \sim 2.5\,\mathrm{Hz}$, high frequency flux loss was estimated to be $10 \sim 20\,\%$, increasing with wind speed and atmospheric stability. Actual uncertainties and biases at our sampling site could be greater due to the distortion of airflow around the building.

Measured OVOC concentrations and fluxes varied significantly with wind direction and time of day. From March to July, the mean nighttime concentration (1σ) of methanol, acetaldehyde, and acetone were 0.46 (0.20), 0.13 (0.02), and 0.39 (0.08) ppb for winds from the sea. Higher concentrations of acetaldehyde and acetone were usually observed during the day, peaking in the direction of a forested park. Methanol concentration did not demonstrate clear diel variability and was often elevated by an order of magnitude under calm conditions or westerly winds. At $\sim 200\,\mathrm{\mu moles\,m^{-2}\,d^{-1}}$, methanol emission was about an order of magnitude larger than those of acetaldehyde and acetone. Both the sign and the magnitude of methanol flux were at odds with the expected air–sea transfer, suggesting large terrestrial emission and possibly anthropogenic influence. Positive correlations were observed between

acetaldehyde flux, acetone flux, and sensible heat flux in the daytime for winds over land, most likely due to emissions from terrestrial plants. From the direction of the sea, however, acetaldehyde flux did not show significant diel difference and largely agreed with the expected sea-to-air transfer. Given its short atmospheric lifetime, the observed nighttime concentration of acetaldehyde was likely sustained in part by marine emission, while contributions from photochemical production appeared to be minor. The small air-to-sea flux of acetone predicted is consistent with only some of the observations.

This coastal environment is spatially patchy and temporally varying, often resulting in inhomogeneous footprints and nonstationary conditions. Even with careful screening of non-ideal sampling conditions, accurate interpretations of measured fluxes are still hampered by the complexity of the surroundings. The analytical methods and qualitative relationships between fluxes presented here should be of greater merit than the absolute magnitudes of the fluxes. To more accurately constrain the air–sea exchange of OVOCs, measurements at sea under more ideal conditions are necessary.

References

Ammann, C., Brunner, A., Spirig, C., and Neftel, A.: Technical note: Water vapour concentration and flux measurements with PTR-MS, Atmos. Chem. Phys., 6, 4643–4651, doi:10.5194/acp-6-4643-2006, 2006.

Apel, E. C., Brauers, T., Koppmann, R., Bandowe, B., Boßmeyer, J. Holzke, C., Tillmann, R., Wahner, A., Wegener, R., Brunner, A., Jocher, M., Ruuskanen, T., Spirig, C., Steigner, D., Steinbrecher, R., Gomez Alvarez, E., Müller, K., Burrows, J. P., Schade, G., Solomon, S. J.,

Ladstätter-Weißenmayer, A., Simmonds, P., Young, D., Hopkins, J. R., Lewis, A. C., Legreid, G., Reimann, S., Hansel, A, Wisthaler, A., Blake, R. S., Ellis, A. M., Monks, P. S., and Wyche, K. P.: Intercomparison of oxygenated volatile organic compound measurements at the SAPHIR atmosphere simulation chamber, J. Geophys. Res., 113, D20307, doi:10.1029/2008JD009865, 2008.

Atkinson, R.: Atmospheric chemistry of VOC and NO_x, Atmos. Environ., 34, 2063–2101, 2000.

Bandy, A. R., Thornton, D. C., Blomquist, B. W., Chen, S., Wade, T. P., Ianni, J. C., Mitchell, G. M., and Nadler, W.: Chemistry of dimethylsulfide in the equatorial Pacific atmosphere, Geophys. Res. Lett., 23, 741–744, 1996.

Bariteau, L., Helmig, D., Fairall, C. W., Hare, J. E., Hueber, J., and Lang, E. K.: Determination of oceanic ozone deposition by ship-borne eddy covariance flux measurements, Atmos. Meas. Tech., 3, 441–455, doi:10.5194/amt-3-441-2010, 2010.

Beale, R., Dixon J., Liss P., and Nightingale P.: Quantification of oxygenated volatile organic compounds in seawater by membrane inlet-proton transfer reaction/mass spectrometry, Anal. Chim. Acta, 706, 128–134, 2011.

Blitz, M. A., Heard, D. E., Pilling, M. J., Arnold, S. R., and Chipperfield M. P.:, Pressure and temperature-dependent quantum yields for the photodissociation of acetone between 279 and 327.5 nm, Geophys. Res. Lett., 31, L06111, doi:10.1029/2003GL018793, 2004.

Blomquist, B. W., Huebert, B. J., Fairall, C. W., and Faloona, I. C.: Determining the sea–air flux of dimethylsulfide by eddy correlation using mass spectrometry, Atmos. Meas. Tech., 3, 1–20, doi:10.5194/amt-3-1-2010, 2010.

Blomquist, B. W., Fairall, C. W., Huebert, B. J., and Wilson, S. T.: Direct measurement of the oceanic carbon monoxide flux by eddy correlation, Atmos. Meas. Tech., 5, 3069–3075, doi:10.5194/amt-5-3069-2012, 2012.

Carpenter, L. J., Lewis, A. C., Hopkins, J. R., Read, K. A., Longley, I. D., and Gallagher, M. W.: Uptake of methanol to the North Atlantic Ocean surface, Global Biogeochem. Cy., 18, GB4027, doi:10.1029/2004GB002294, 2004.

Davison, B., Taipale, R., Langford, B., Misztal, P., Fares, S., Matteucci, G., Loreto, F., Cape, J. N., Rinne, J., and Hewitt, C. N.: Concentrations and fluxes of biogenic volatile organic compounds above a Mediterranean macchia ecosystem in western Italy, Biogeosciences, 6, 1655–1670, doi:10.5194/bg-6-1655-2009, 2009.

de Gouw, J., Warneke, C., Karl, T., Eerdekens, G., van der Veen, C., and Fall, R.: Sensitivity and specificity of atmospheric trace gas detection by proton-transfer-reaction mass spectrometry, Int. J. Mass Spectrom., 223–224, 365–382, 2003.

de Gouw, J., Warneke, C., Holzinger, R., Klupfel, T., and Williams, J.: Inter-comparison between airborne measurements of methanol, acetonitrile and acetone using two differently configured PTR-MS instruments, Int. J. Mass Spectrom., 239, 129–137, 2004.

Duce, R. A., Liss, P., Merrill, J. T., Atlas, E. L., Buat-Menard, P., Hicks, B. B., Miller, J. M., Prospero, J. M., Arimoto, R., Church, T. M., Ellis, W., Galloway, J. N., Hansen, L., Jickells, T. D., Knap, A. H., Reinhardt, K. H., Schneider, B., Soudine, A., Tokos, J. J., Tsunogai, S., Wollast, R., and Zhou, M.: The atmospheric input of trace species to the world ocean, Global Biogeochem. Cy., 5, 193–259, 1991.

Duncan, B. N., Logan, J. A., Bey, I., Megretskaia, I. A., Yantosca, R. M., Novelli, P. C., Jones, N. B., and Rinsland, C. P.: Global budget of CO, 1988–1997: source estimates and validation with a global model, J. Geophys. Res., 112, D22301, doi:10.1029/2007JD008459, 2007.

Fairall, C. W., Hare, J. E., Edson, J. B., and McGillis, W.: Parameterization and micrometeorological measurements of air–sea gas transfer, Bound.-Lay. Meteorol., 96, 63–105, 2000.

Fairall, C. W., Bradley, E. F., Hare, J. E., Grachev, A. A., and Edson J. B.: Bulk parameterization of air–sea fluxes: updates and verification for the COARE algorithm, J. Climate, 16, 571–591, 2003.

Fairall, C. W., Yang, M., Bariteau, L., Edson, J. B., Helmig, D., McGillis, W., Pezoa, S., Hare, J. E., Huebert, B., and Blomquist, B.: Implementation of the coupled ocean-atmosphere response experiment flux algorithm with CO_2, dimethyl sulfide, and O_3, J. Geophys. Res., 116, C00F09, doi:10.1029/2010JC006884, 2011.

Fischer, E. V., Jacob, D. J., Millet, D. B., Yantosca, R. M, and Mao, J.: The role of the ocean in the global atmospheric budget of acetone, Geophys. Res. Lett., 39, L01807, doi:10.1029/2011GL050086, 2012.

Grant, A., Yates, E. L., Simmonds, P. G., Derwent, R. G., Manning, A. J., Young, D., Shallcross, D. E., and O'Doherty, S.: A five year record of high-frequency in situ measurements of non-methane hydrocarbons at Mace Head, Ireland, Atmos. Meas. Tech., 4, 955–964, doi:10.5194/amt-4-955-2011, 2011.

Griessbaum F. and Schmidt, A.: Advanced tilt correction from flow distortion effects on turbulent CO_2 fluxes in complex environments using large eddy simulation, Q. J. R. Meteorol. Soc., 135, 1603–1613, doi:10.1002/qj.472, 2009.

Goebbert D. J. and Wentold P. G.: Water dimer proton affinity from the kinetic method: dissociation energy of the water dimer, Eur. J. Mass. Spectrom.,10, 837–846, 2004.

Guenther, A., Geron, C., Pierce, T., Lamb, B., Harley, P., and Fall, R.: Natural emissions of non-methane volatile organic compounds; carbon monoxide, and oxides of nitrogen from North America, Atmos. Environ., 34, 2205–2230, 2000.

Heikes, B. G., Chang, W. N., Pilson, M. E. Q., Swift, E., Singh, H. B., Guenther, A., Jacob, D. J., Field, B. D., Fall, R., Riemer, D., and Brand, L.: Atmospheric methanol budget and ocean implication, Global Biogeochem. Cy., 16, 1133, doi:10.1029/2002GB001895, 2002.

Horst, T. W. and Weil, J. C.: Footprint estimation for scalar flux measurements in the atmospheric surface layer, Bound.-Lay. Meteorol., 59, 279–296, 1992.

Hu, L., Millet, D. B., Mohr, M. J., Wells, K. C., Griffis, T. J., and Helmig, D.: Sources and seasonality of atmospheric methanol based on tall tower measurements in the US Upper Midwest, Atmos. Chem. Phys., 11, 11145–11156, doi:10.5194/acp-11-11145-2011, 2011.

Jacob, D. J., Field, B. D., Jin, E. M., Bey, I., Li, Q., Logan, J. A., Yantosca, R. M., and Singh H. B.: Atmospheric budget of acetone, J. Geophys. Res., 107, 4100, doi:10.1029/2001JD000694, 2002.

Jacob, D. J., Field, B. D., Li, Q. B., Blake, D. R., de Gouw, J., Warneke, C., Hansel, A., Wisthaler, A., Singh, H. B., and Guenther, A.: Global budget of methanol: constraints from atmospheric observations, J. Geophys. Res., 110, D08303, doi:10.1029/2004JD005172, 2005.

Jardine, K., Harley, P., Karl, T., Guenther, A., Lerdau, M., and Mak, J. E.: Plant physiological and environmental controls over the exchange of acetaldehyde between forest canopies and the atmosphere, Biogeosciences, 5, 1559–1572, doi:10.5194/bg-5-1559-2008, 2008.

Kaimal, J., Wyngaard, J., Izumi, Y., and Coté, O.: Spectral characteristics of surface layer turbulence, Q. J. R. Meteorol. Soc., 98, 563–589, doi:10.1002/qj.49709841707, 1972.

Karl, T., Guenther, A., Lindinger, C., Jordan, A., Fall, R., and Lindinger, W.: Eddy covariance measurements of oxygenated volatile organic compound fluxes from crop harvesting using a redesigned proton-transfer-reaction mass spectrometer, J. Geophys. Res., 106, 24157–24167, doi:10.1029/2000JD000112, 2001.

Karl, T. G., Spirig, C., Rinne, J., Stroud, C., Prevost, P., Greenberg, J., Fall, R., and Guenther, A.: Virtual disjunct eddy covariance measurements of organic compound fluxes from a subalpine forest using proton transfer reaction mass spectrometry, Atmos. Chem. Phys., 2, 279–291, doi:10.5194/acp-2-279-2002, 2002.

Karl, T., Potosnak, M., Guenther, A., Clark, D., Walker, J., Herrick, J. D., and Geron, C.: Exchange processes of volatile organic compounds above a tropical rain forest: implications for modeling tropospheric chemistry above dense vegetation, J. Geophys. Res., 109, D18306, doi:10.1029/2004JD004738, 2004.

Kljun, N., Calanca, P., Rotach, M. W., and Schmid H. P.: A simple parameterisation for flux footprint predictions, Bound.-Lay. Meteorol., 112, 503–523, 2004.

Langford, B., Davison, B., Nemitz, E., and Hewitt, C. N.: Mixing ratios and eddy covariance flux measurements of volatile organic compounds from an urban canopy (Manchester, UK), Atmos. Chem. Phys., 9, 1971–1987, doi:10.5194/acp-9-1971-2009, 2009.

Lewis, A. C., Hopkins, J. R., Carpenter, L. J., Stanton, J., Read, K. A., and Pilling, M. J.: Sources and sinks of acetone, methanol, and acetaldehyde in North Atlantic marine air, Atmos. Chem. Phys., 5, 1963–1974, doi:10.5194/acp-5-1963-2005, 2005.

Lindinger, W., Hansel A., and Jordan, A.: On-line monitoring of volatile organic compounds at pptv levels by means of Proton-Transfer-Reaction Mass Spectrometry (PTR-MS), medical applications, food control and environmental research, Int. J. Mass Spectrom. Ion Proc., 173, 191–241, 1998.

Liss, P. S. and Slater, P. G.: Flux of gases across the air–sea interface, Nature, 247, 181–184, doi:10.1038/247181a0, 1974.

Madronich, S. and Calvert, J. G.: Permutation reactions of organic peroxy radicals in the troposphere, J. Geophys. Res., 95, 5697–5715, 1990.

Marandino, C. A., De Bruyn, W. J., Miller, S. D., Prather, M. J., and Saltzman, E. S.: Oceanic uptake and the global atmospheric acetone budget, Geophys. Res. Lett., 32, L15806, doi:10.1029/2005GL023285, 2005.

Millet, D. B., Jacob, D. J., Turquety, S., Hudman, R. C., Wu, S., Fried, A., Walega, J., Heikes, B. G., Blake, D. R., Singh, H. B., Anderson, B. E., and Clarke, A. D.: Formaldehyde distribution over North America: Implications for satellite retrievals of formaldehyde columns and isoprene emission, J. Geophys. Res., 111, D24S02, doi:10.1029/2005JD006853, 2006.

Millet, D. B., Jacob, D. J., Custer, T. G., de Gouw, J. A., Goldstein, A. H., Karl, T., Singh, H. B., Sive, B. C., Talbot, R. W., Warneke, C., and Williams, J.: New constraints on terres-

trial and oceanic sources of atmospheric methanol, Atmos. Chem. Phys., 8, 6887–6905, doi:10.5194/acp-8-6887-2008, 2008.

Moore, C. J.: Frequency response correction for eddy correlation systems, Bound.-Lay. Meteorol., 37, 17–35, 1986.

Nemecek-Marshall, M., Macdonald, R. C., Franzen, F. J., Wojciechowski, C. L., and Fall, R.: Methanol emission from leaves – enzymatic detection of gas-phase methanol and relation of methanol fluxes to stomatal conductance and leaf development, Plant Physiol., 108, 1359–1368, 1995.

Northway, M., de Gouw, J., Fahey, D., Gao, R., Warneke, C., Roberts, J., and Flocke, F.: Evaluation of the role of heterogeneous oxidation of alkenes in the detection of atmospheric acetaldehyde, Atmos. Environ., 38, 6017–6028, 2004.

Oncley, S. P.: Flux Parameterisation Techniques in the Atmospheric Surface Layer, Ph.D. thesis, Univ. of California, Irvine, 202 pp., 1989.

Panin G. N., Tetzlaff, G., and Raabe, A.: Inhomogeneity of the land surface and problem in parametrization of the surface fluxes in natural conditions, Theor. Appl. Climatol., 60, 163–178, 1998.

Raabe, A., Arnold, K., and Ziemann, A.: Horizontal turbulent fluxes of sensible heat and horizontal homogeneity in micrometeorological experiments. J. Atmos. Oceanic Technol., 19, 1225–1230. doi:10.1175/1520-0426(2002)019<1225:HTFOSH>2.0.CO;2, 2002.

Rinne, H. J. I., Guenther, A. B., Warneke, C., de Gouw, J. A., and Luxembourg, S. L.: Disjunct eddy covariance technique for trace gas flux measurements, Geophys. Res. Lett., 28, 3139–3142, doi:10.1029/2001GL012900, 2001.

Roberts, J. M.: The atmospheric chemistry of organic nitrates, Atmos. Environ., 24, 243–287, 1990.

Salisbury, G., Rickard, A. R., Monks, P. S., Allan, B. J., Bauguitte, S., Penkett, S. A., Carslaw, N., Lewis, A. C., Creasey, D. J., Heard, D. E., Jacobs, P. J., and Lee, J. D.: Production of peroxy radicals at night via reactions of ozone and the nitrate radical in the marine boundary layer, J. Geophys. Res., 106, 12669–12687, doi:10.1029/2000JD900754, 2001.

Sander, S. P., Golden, D. M., Kurylo, M. J., Moortgat, G. K., Wine, P. H., Ravishankara, A. R., Kolb, C. E., Molina, M. J., Finlayson-Pitts, B. J., Huie, R. E., and Orkin, V. L.: Chemical Kinetics and Photochemical Data for Use in Atmospheric Studies, Evaluation Number 15, Jet Propulsion Laboratory, Pasadena, CA, USA, online available at: http://jpldataeval.jpl.nasa.gov/ (last access: August 2012), 2006.

Schmid, H. P.: Source areas for scalars and scalar fluxes. Bound.-Lay. Meteorol. 67, 293–318, 1994.

Schulz E. W. and Sanderson, B. G.: Stationarity of turbulence in light winds during the maritime continent thunderstorm experiment, Bound.-Lay. Meteorol., 111, 523–541, 2004.

Sinha, V., Williams, J., Meyerhöfer, M., Riebesell, U., Paulino, A. I., and Larsen, A.: Air-sea fluxes of methanol, acetone, acetaldehyde, isoprene and DMS from a Norwegian fjord following a phytoplankton bloom in a mesocosm experiment, Atmos. Chem. Phys., 7, 739–755, doi:10.5194/acp-7-739-2007, 2007.

Singh, H. B., O'Hara, D., Herlth, D., Sachse, W., Blake, D. R., Bradshaw, J. D., Kanakidou, M., and Crutzen, P. J.: Acetone in the atmosphere: distribution, sources and sinks, J. Geophys. Res., 99, 1805–1819, 1994.

Singh, H. B., Kanakidou, M., Crutzen, P. J., and Jacob, D. J.: High concentrations and photochemical fate of oxygenated hydrocarbons in the global troposphere, Nature, 378, 50–54, 1995.

Singh, H., Chen, Y., Tabazadeh, A., Fukui, Y., Bey, I., Yantosca, R., Jacob, D., Arnold, F., Wohlfrom, K., Atlas, E., Flocke, F., Blake, D., Blake, N., Heikes, B., Snow, J., Talbot, R., Gregory, G., Sachse, G., Vay, S., and Kondo, Y.: Distribution and fate of selected oxygenated organic species in the troposphere and lower stratosphere over the Atlantic, J. Geophys. Res., 105, 3795–3805, 2000.

Singh, H. B., Salas, L. J., Chatfield, R. B., Czech, E., Fried, A., Walega, J., Evans, M. J., Field, B. D., Jacob, D. J., Blake, D., Heikes, B., Talbot, R., Sachse, G., Crawford, J. H., Avery, M. A., Sandholm, S., and Fuelberg, H.: Analysis of the atmospheric distribution, sources, and sinks of oxygenated volatile organic chemicals based on measurements over the Pacific during TRACE-P, J. Geophys. Res., 109, D15S07, doi:10.1029/2003JD003883, 2004.

Spirig, C., Neftel, A., Ammann, C., Dommen, J., Grabmer, W., Thielmann, A., Schaub, A., Beauchamp, J., Wisthaler, A., and Hansel, A.: Eddy covariance flux measurements of biogenic VOCs during ECHO 2003 using proton transfer reaction mass spectrometry, Atmos. Chem. Phys., 5, 465–481, doi:10.5194/acp-5-465-2005, 2005.

Taddei, S., Toscano, P., Gioli, B., Matese, A., Miglietta, F., Vaccari, F. P., Zaldei, A., Custer, T., and Williams, J.: Carbon dioxide and acetone air–sea fluxes over the Southern Atlantic, Environ. Sci. Technol., 43, 5218–5222, 2009.

Taipale, R., Ruuskanen, T. M., Rinne, J., Kajos, M. K., Hakola, H., Pohja, T., and Kulmala, M.: Technical Note: Quantitative long-term measurements of VOC concentrations by PTR-MS

– measurement, calibration, and volume mixing ratio calculation methods, Atmos. Chem. Phys., 8, 6681–6698, doi:10.5194/acp-8-6681-2008, 2008.

Warneke, C., Karl, T., Judmaier, H., Hansel, A., Jordan, A., Lindinger, W., and Crutzen, P. J.: Acetone, methanol, and other partially oxidized volatile organic emissions from dead plant matter by abiological processes: significance for atmospheric HO_x chemistry, Global Bio-geochem. Cy., 13, 9–17, 1999.

Warneke, C., Luxembourg, S. L., de Gouw, J. A., Rinne, H. J. I., Guenther, A. B., and Fall, R.: Disjunct eddy covariance measurements of oxygenated volatile organic compounds fluxes from an alfalfa field before and after cutting, J. Geophys. Res., 107, 4067, doi:10.1029/2001JD000594, 2002.

Warneke, C., de Gouw, J. A., Kuster, W. C., Goldan, P. D., and Fall, R.: Validation of atmospheric VOC measurements by proton-transfer-reaction mass spectrometry using a gas chromato-graphic preseparation method, Environ. Sci. Technol., 37, 2494–2501, 2003.

Williams, J., Holzinger, R., Gros, V., Xu, X., Atlas, E., and Wallace D. W. R.: Measurements of organic species in air and seawater from the tropical Atlantic, Geophys. Res. Lett., 31, L23S06, doi:10.1029/2004GL020012, 2004.

Wilson, J. D. and Swaters, G. E.: The source area influencing a measurement in the planetary boundary layer: the "footprint" and the "distribution of contact distance", Bound.-Lay. Meteorol., 55, 25–46, 1991.

World Meteorological Organization: Initial guidance to obtain representative meteorological observations at urban sites, Instruments and observing methods, Report No. 81, WMO/TD-No. 1250, Geneva, 47 pp., 2006.

Wróblewski, T., Ziemczonek, L., Alhasan, A. M., and Karwasz, G. P.: Ab initio and density functional theory calculations of proton affinities for volatile organic compounds, Eur. Phys. J., 144, 191–195, doi:10.1140/epjst/e2007-00126-7, 2007.

Yang, M., Blomquist, B. W., and Huebert, B. J.: Constraining the concentration of the hydroxyl radical in a stratocumulus-topped marine boundary layer from sea-to-air eddy covariance flux measurements of dimethylsulfide, Atmos. Chem. Phys., 9, 9225–9236, doi:10.5194/acp-9-9225-2009, 2009.

Yang, M., Blomquist, B. W., Fairall, C. W., Archer, S. D., and Huebert, B. J.: Air-sea exchange of dimethylsulfide in the Southern Ocean: measurements from SO GasEx compared to temperate and tropical regions, J. Geophys. Res., 116, C00F05, doi:10.1029/2010JC006526, 2011.

Zhou, X. and Mopper, K.: Carbonyl compounds in the lower marine troposphere over the Caribbean Sea and Bahamas, J. Geophys. Res.-A., 98, 2385–2392, 1993.

Zhao, J. and Zhang, R. Y.: Proton transfer reaction rate constants between hydronium ion ($H_3O^{(+)}$) and volatile organic compounds, Atmos. Environ., 38, 2177–2185, 2004.
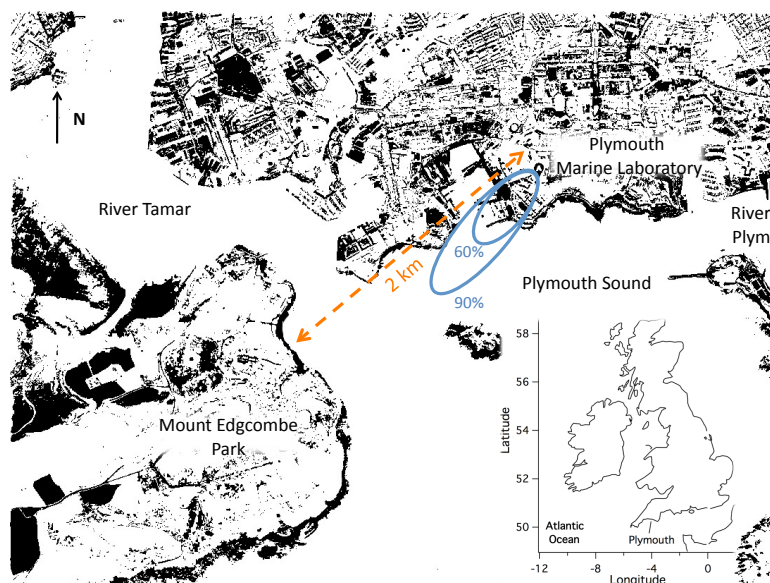
Fig. 1. Map of the Plymouth Sound and the location of Plymouth. The small and large ellipses illustrate the approximated 60 % and 90 % (cumulative) flux footprint under typical conditions. At ~ 2 km SW of the PLM and separated by the River Tamar, the forested Mount Edgcombe Park likely lies outside of the flux footprint.
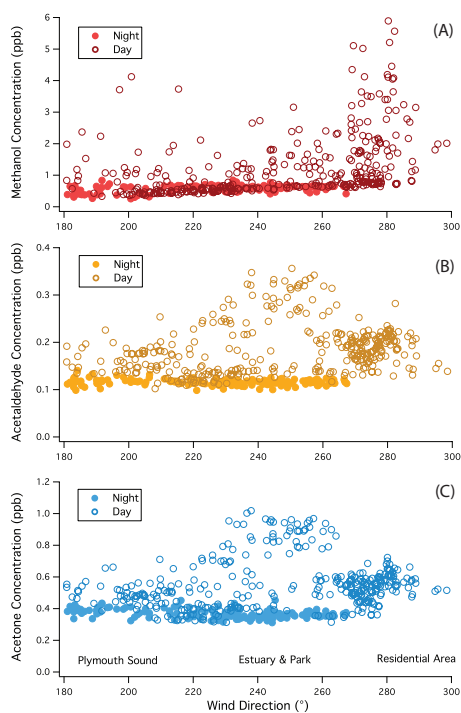
Fig. 2. Concentrations of methanol **(A)**, acetaldehyde **(B)**, and acetone **(C)** as a function of wind direction during 6 ~ 8 June. For acetaldehyde and acetone, concentrations were higher during the day than at night and demonstrated maxima in the direction of WSW (Mount Edgcombe park). Much higher methanol concentrations were observed during the day and typically from the NW, possibly due to anthropogenic emission.
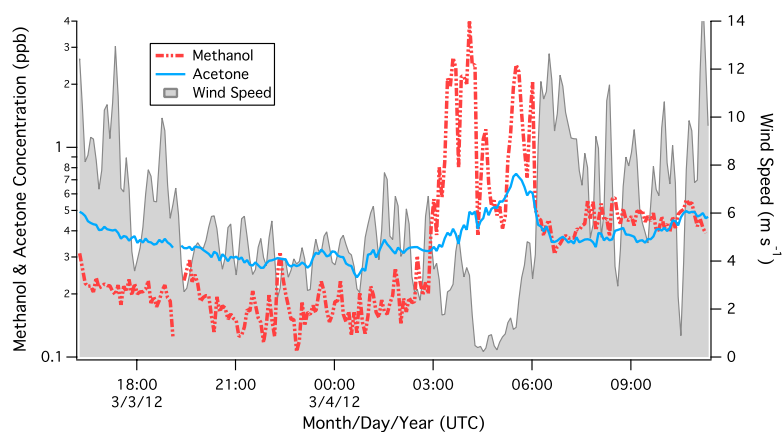
Fig. 3. Concentrations of methanol and acetone during 3 ~ 4 March, along with wind speed (from SW). Greater fluctuations were apparent in the concentration of methanol than in acetone on short timescales, in part due to greater spatial heterogeneity of methanol sources. Methanol concentration increased by an order of magnitude when the wind ceased, likely due to a shallow nocturnal boundary layer.
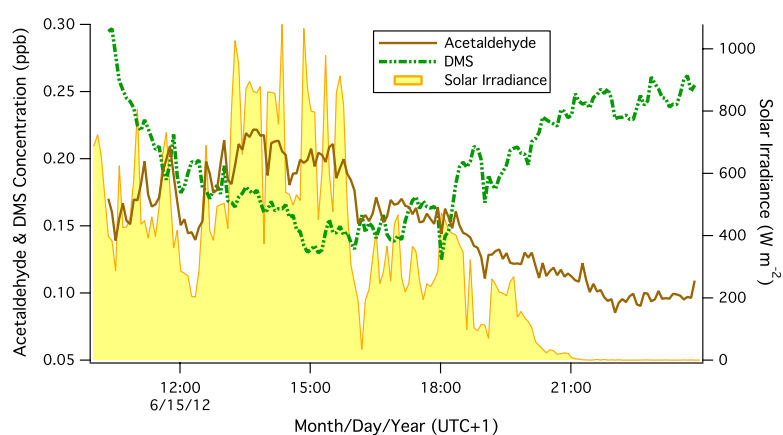
Fig. 4. Concentrations of acetaldehyde and DMS on 15 June, along with solar irradiance. With strong winds from SSW (over the Plymouth Sound), DMS concentration was detectable by the PTR-MS and demonstrated the expected diel variability, while acetaldehyde concentration peaked in solar noon and declined for the rest of the daytime.
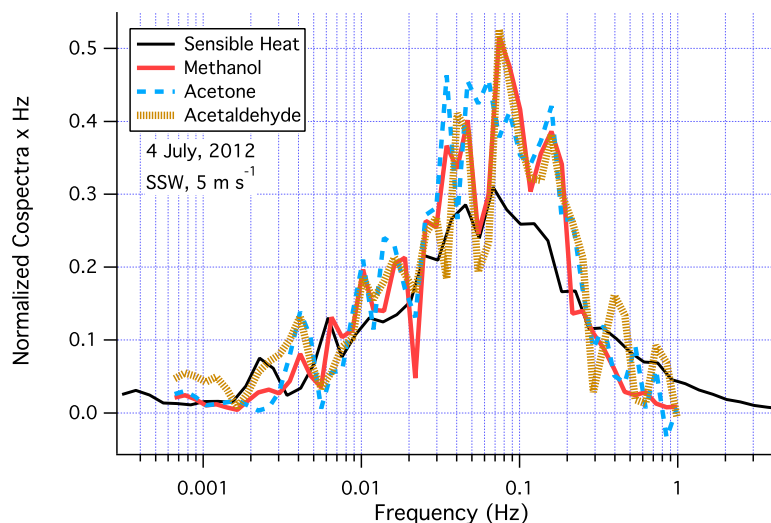
Fig. 5. Cospectra of sensible heat, methanol, acetone, and acetaldehyde normalized to the respective fluxes during 4 h of steady winds on 4 July. Trimming of plants immediately upwind resulted in exceptionally large fluxes and well-defined cospectra for all three OVOC species, which showed good agreement with each other.
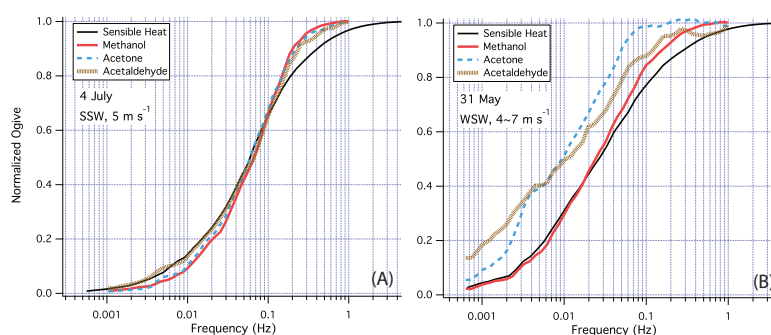
Fig. 6. Ogive of sensible heat, methanol, acetone, and acetaldehyde normalized to the respective fluxes for 4 July **(A)** and 31 May **(B)**. On 4 July (same period as Fig. 5), the ogives of different OVOCs demonstrated good agreement with each other and to that of sensible heat due to strong local emissions and steady winds. In contrast, rising winds on 31 May caused increasing concentrations of acetone and acetaldehyde, which is evident in the greater ogives at low frequencies.
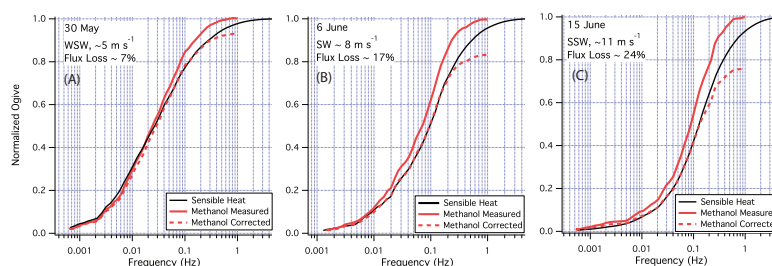
Fig. 7. Ogives of sensible heat and methanol (before and after attenuation correction) for three days of different wind speeds and atmospheric stability. Flux loss at high frequencies increased with wind speed and stability, where a greater contribution to the flux came from smaller eddies.

8145
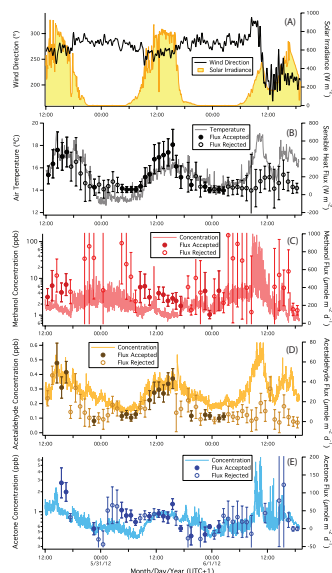
Fig. 8. Time series of wind direction and solar irradiance **(A)**, temperature and sensible heat flux **(B)**, methanol concentration and flux **(C)**, acetaldehyde concentration and flux **(D)**, and acetone concentration and flux **(E)** from 30 May to 1 June, three sunny days with mostly light to moderate breeze from land. Methanol concentration increased by over an order of magnitude when the winds ceased, while acetaldehyde and acetone concentrations were generally higher during the day than at night. Many hours of fluxes did not pass the quality control criteria because of excessive variability in wind direction.
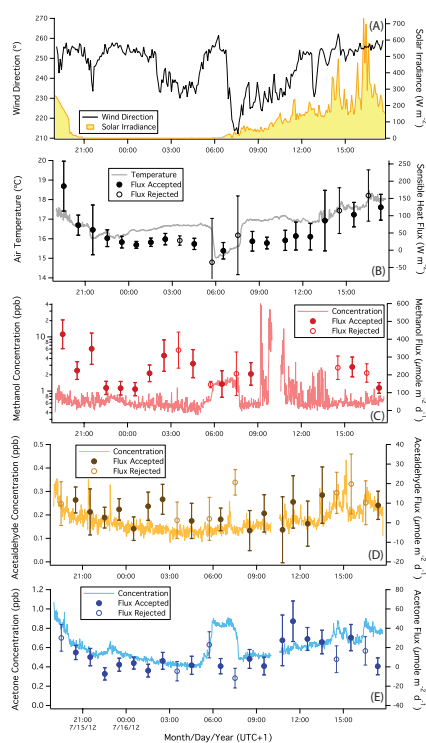
8146
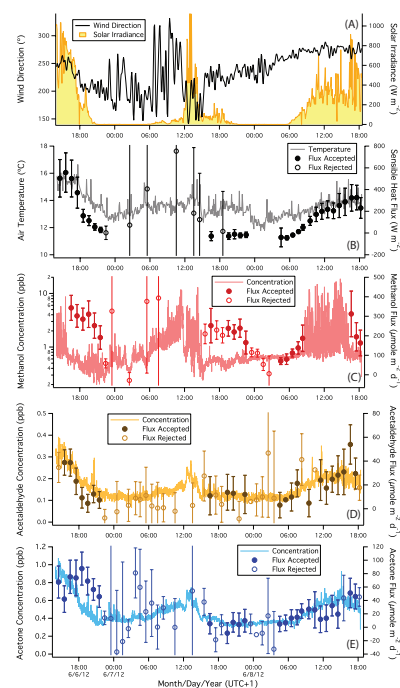
Fig. 9. As with Fig. 8, but for 6 ∼ 8 June. During this windy period, acetaldehyde and acetone fluxes as well as concentrations were higher during the day, following the trend of heat flux. Acceptable flux measurements could not be made for most of 7 June and a few hours on 8 June due to corruption of the sonic anemometer data in the presence of heavy rain.

**Fig. 10.** As with Fig. 8 and 9, but for 15 ∼ 16 July. Fluxes varied noticeably with wind direction, reflecting an inhomogeneous footprint. A rapid change in wind direction at ∼ 06:00 LT on 16 July brought along lower temperature and much higher methanol and acetone concentrations. Fluxes were rejected during such periods of highly variable conditions for violation of the stationarity assumption.
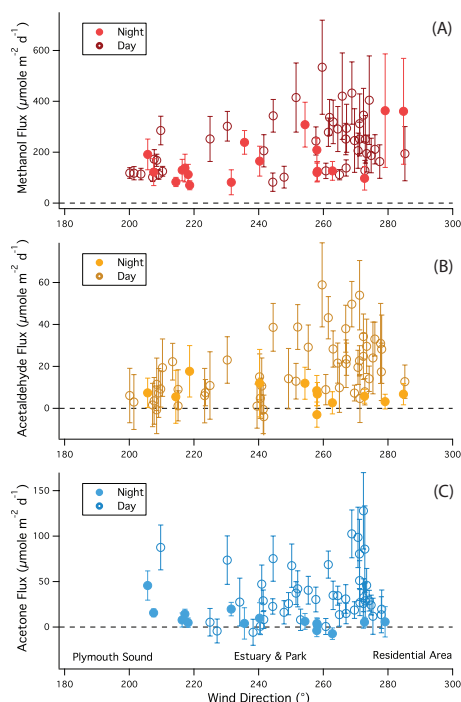
Fig. 11. Hourly fluxes of methanol **(A)**, acetaldehyde **(B)**, and acetone **(C)** from March to July. Methanol fluxes were large and always positive, peaking in the direction of WSW. For acetaldehyde, fluxes from the direction of the Plymouth Sound were slightly positive and demonstrated little difference between day and night. Acetone flux was lower at night than during the day, and occasionally negative.
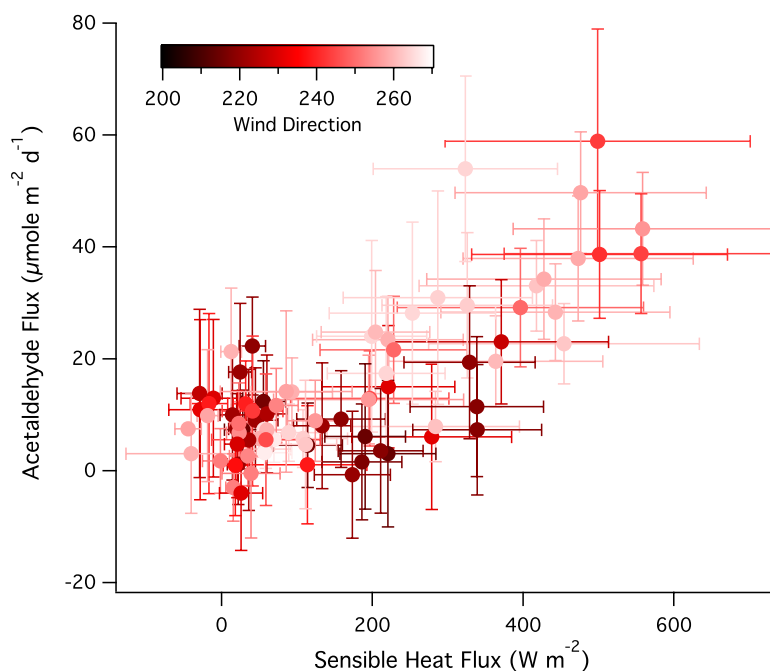
Fig. 12. Acetaldehyde flux vs. heat flux from March to July, color-coded by wind direction. When winds were coming from SW to W, a strong positive correlation was observed between the two fluxes ($r^2 = 0.72$), likely as a result of terrestrial plant emission. With SSW winds, though, acetaldehyde flux was generally lower and demonstrated no clear relationship with heat flux, suggesting possible oceanic emission.
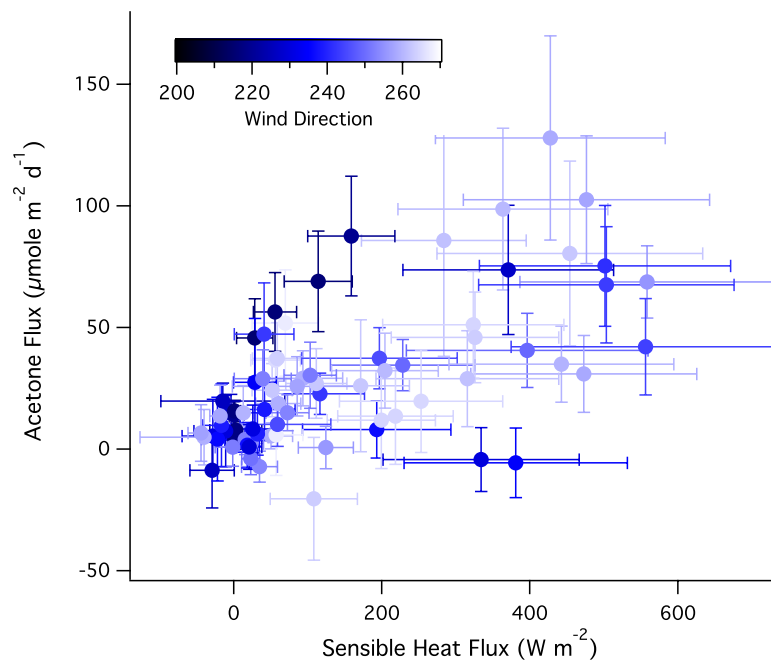
Fig. 13. Acetone flux vs. heat flux from March to July, color-coded by wind direction. A positive correlation was sometimes observed between the two fluxes, such as when winds were from the west ($r^2 = 0.52$).
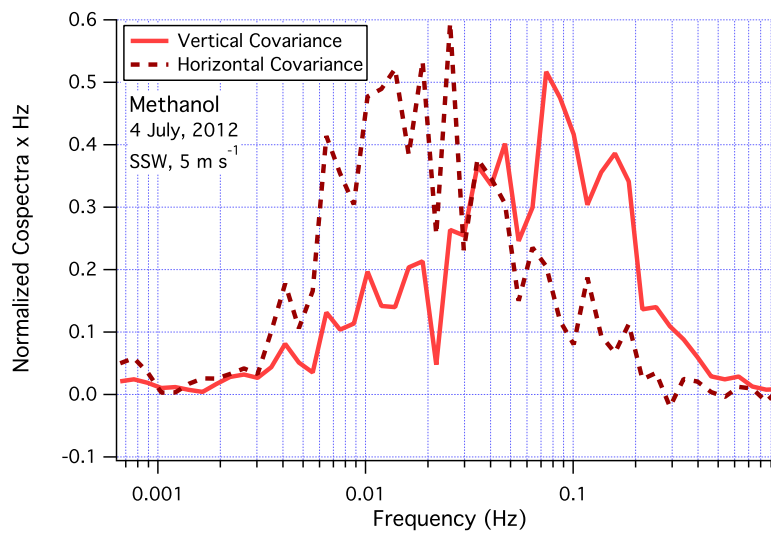
Fig. 14. Normalized methanol cospectra for vertical covariance (same as Fig. 5) and horizontal covariance on 4 July. The horizontal cospectrum peaked at a lower frequency than the vertical cospectrum, likely related to spatial inhomogeneity.